Investigation of Performance, Loads, and Vibrations of a Coaxial Helicopter in High Speed-Flight

George Jacobellis
Graduate Research Assistant
Rensselaer Polytechnic Institute
Troy, New York, USA

Farhan Gandhi
Professor
Rensselaer Polytechnic Institute
Troy, New York, USA

ABSTRACT

A lift-offset coaxial helicopter is simulated using the Rotorcraft Comprehensive Analysis System (RCAS) at a speed of 230 kts. The XH-59 Advancing Blade Concept demonstrator aircraft is used for the simulation model. A variety of trim states are explored by varying vehicle pitch attitude and redundant controls, such as main rotor speed and differential lateral pitch. The performance, vibrations, and blade loads are compared for different trim states, notably, those states utilizing negative rotor power to drive the propulsor and states in which the rotor power is constrained to be non-negative. The optimal trim state for a system with a powered or free spinning rotor lies at about 3°pitch attitude, while the optimal trim state for a vehicle in which the rotor can extract power and direct it to the propulsor lies at 6-7°pitch attitude. With the aircraft operating at a high pitch attitude, the horizontal tail is able to provide a significant amount of the necessary aircraft lift, while the rotor can provide the longitudinal moment necessary for trim. The Blade loads and hub vibrations for the negative rotor power state are similar or less than for the marginally powered state.

NOTATION

(x,y,z)	Vehicle coordinate system, oriented positive (aft, starboard, up)
A	Longitudinal trim variable
B	Lateral trim variable
D	Drag
F	Rotor force
H	Rotor longitudinal force, positive aft
LOS	Lift-offset (%)
M	Rotor moment
P	Power
R	Rotor radius
T	Rotor thrust
T_{prop}	Propulsor Thrust
V_∞	Freestream velocity
ψ	Rotor azimuth angle
η_p	Propeller efficiency
θ	Blade pitch angle
Γ	Rotor phase angle
$()_U$	Upper rotor quantity
$()_L$	Lower rotor quantity
$()_0$	Collective component
$()_{1C}$	Longitudinal component
$()_{1S}$	Lateral component
$()_3$	3/rev component
$()'$	Differential trim variable

Presented at the AHS 72nd Annual Forum, West Palm Beach, Florida, May 17–19, 2016.

INTRODUCTION

There is currently a large interest in developing rotorcraft platforms that can achieve high speeds while not sacrificing hover efficiency. The U.S. Department of Defense has put fourth a strategic plan known as the Future Vertical Lift, with the objective of developing a fleet of next generation air vehicles. The first step in this plan is a technology demonstration program known as the Joint Multi-Role Technology Demonstration (JMR TD). This program is currently funding the construction of two air vehicle demonstrators, the Bell Valor tilt rotor, and the Sikorsky-Boeing Defiant lift-offset compound. The target speed for the JMR TD is 230 kt. While tilt rotors excel at reaching high speeds (The Valor has a cruise target of 280 kt) (Ref. 1), they have the inherent drawback of having to use the same rotors for hover as well as propulsion in forward flight. This forces compromises to be made in the rotor design, resulting in rotors that have high disk loading relative to conventional hovering rotors, and high inertia compared to conventional propellers. The high inertia of the propellers in forward flight requires a very stiff and heavy wing to prevent whirl-flutter instability (Ref. 2).

Edgewise rotors have their own problems at high speeds; stall on the retreating blades and drag divergence on the advancing tips lead to high vibrations and large drag as flight speed increases. There are several options for avoiding these problems. Slowing the rotor can allow the helicopter to reach very high speeds while keeping the advancing blade tips below the drag divergence Mach number. Slowing the rotor becomes a problem for conventional helicopters as the retreating blades experience very low dynamic pressure and reverse

flow and cannot produce the forces and moments necessary to balance the helicopter. The slowed rotor can be partially offloaded on the retreating sides, as is the case with lift-offset coaxial configurations, or on both sides by incorporating a lifting wing. In these configurations it is not necessary for the retreating side to produce a significant amount of lift and the helicopter can easily fly at high advance ratios.

While conventional helicopters must tilt forward to provide a propulsive force, the use of dedicated auxiliary propulsion, usually a small pusher propeller, can provide this propulsive force with higher efficiency. With an auxiliary propulsor, a rotor can be made to tilt aft, with the aircraft's forward speed creating an upwash through the rotor and reducing the rotor power required to zero or even negative values.

Coaxial lift-offset helicopters were pioneered by Sikorsky with the XH-59 Advancing Blade Concept (ABC) demonstrator. The XH-59 reached speeds in excess of 250 kts, but rotor aerodynamics at those speeds led to large drag and high vibrations (Refs. 3–9). Sikorsky has since made a great deal of progress in this arena by improving the rotor aerodynamics and using active vibration control, which have proven to be effective on the X2 Technology^{TM} Demonstrator (Refs. 10–13) and the S-97 raider. The most notable improvements are the use of 4 bladed rotors, rather than the 3 on the XH59; reduced twist and chord on the inboard sections, which helps reduce drag in high speed; and double ended airfoils on the inboard sections, which also reduce drag in the reverse flow region. The Defiant has a target speed of 250 kt and will also incorporate a variable RPM drive system; it is scheduled to fly in 2017 (Ref. 1).

The inclusion of a variable RPM drive system is an indication that engineers wish to slow the rotor to previously unreached speeds, and fly at increasingly high advance ratios. As the rotor slows, its required power decreases, possibly even decreasing to negative values. Previous aircraft, such as the X2TD, had a clutched rotor that was incapable of operating the rotor in negative power states. The X2 would therefore fly with zero or slightly positive rotor power. Future aircraft will have a geared connection to the propeller that is able to operate the rotor in a negative power state, such that the rotor torque will help to drive the propeller.

In addition to Sikorsky, interest in coaxial helicopters has spread to a number of other researchers. At the University of Maryland, A group led by Leishman has used Blade Element Momentum Theory to develop optimum coaxial rotors in hover and axial flight conditions. (Refs. 14, 15). More recently, Hersey et. al. performed multi-objective optimization of coaxial rotors in hover and forward flight using free vortex wake (Ref. 16). Rand and Khromov carried out a similar optimization in Ref. (Ref. 17). Also at The University of Maryland, Schmaus and Chopra used UMARC to analyze the blade loads and performance of a coaxial rotor (Ref. 18) and Passe et. al. modeled an X2 like aircraft with high fidelity CFD and identified important aerodynamic interactions between the rotor and the fuselage and tail surfaces. These studies were limited, however, in that they constrained the rotor speed and vehicle pitch to specific values.

Giovanetti and Hall, have undertaken similar efforts in optimization of coaxial helicopters, starting with Refs. 19 and 20, and have recently expanded their study to include multipoint optimization (Ref. 21). In Refs. 20, 21 Giovanetti and Hall are able to use formal optimization techniques to attain blade twist and chord distributions very similar to that of the X2. Higher Harmonic control is also incorporated into the optimization. Although Ref. 20 did compare optimized trim solutions with different levels of propulsive thrust and at different pitch attitudes, it did not include conditions in which the rotor was significantly slowed, in autorotation, or negative power states.

Johnson used CAMRAD II to study the performance and maximum loading capability of high speed coaxial helicopters (Refs. 22, 23). Johnson highlighted the importance of lift offset and its ability to increase performance and maximum loading at a given rotor speed. Slowed rotors were examined in Refs. 24 and 25 where Floros and Johnson showed that slowed rotors produced less drag and could remain stable at high advance ratios.

Kim and Brown at the University of Glasgow conducted a high fidelity analysis of a coaxial helicopter using the vorticity transport method (Ref. 26), and also investigated aerodynaim interactions in Ref. 27. Ferguson and Thompson investigated performance and flight dynamics of coaxial helicopters in Refs. 28 and 29.

While many studies focused on optimizing coaxial rotors or accurately analyzing certain phenomena, the current study focuses on how the redundant controls of a coaxial helicopter can be used. Because redundant controls offer numerous different trim states, they can be used to improve performance, noise, vibrations, or loads (Refs. 30–35). Ref. 36 describes how coaxial helicopters can vary the rotor speed and differential collective to achieve performance benefits. The current study improves upon the work done in Ref. 36 by improving the simulation model from a dynamic wake to a prescribed wake and expanding the scope of the results to higher pitch attitudes and lower rotor speeds.

COAXIAL SIMULATION MODEL

A model of the XH-59 has been developed in the Rotorcraft Comprehensive Analysis System (RCAS) (Ref. 37) with the technical specifications for the aircraft from Felker, Rudell, and Pleasents (Refs. 4, 5, 8). Key properties are summarized in Table 1.

Controls

The XH-59 employs two counter rotating rotors, the upper rotor rotating counter-clockwise and the lower rotating clockwise. Each of the two rotors can independently vary collective and cyclic pitch. This gives the rotor system a total of six degrees of freedom. $\theta_{0U}, \theta_{1CU}, \theta_{1SU}, \theta_{0L}, \theta_{1CL}, \theta_{1SL}$, where the subscripts U and L correspond to the upper and lower rotors,

Table 1. XH-59 Aircraft Characteristics

Rotor engines	2 P&W PT6T-3 turboshaft
Propulsor thrust engines	2 P&W J60-P-3A turbojet
Fuselage length	40.8 ft
Overall height	12.9 ft
Rotor diameter	36 ft
Rotor separation	2.5 ft
Shaft tilt	0°
Rotor (lower)	5.3in aft, 3 ft above CG
Engine attachment	2.1ft fwd, 1ft below CG
Nominal rotor speed	345 RPM
Nominal rotor tip speed	650 ft/sec
Blades per rotor	3
Blade precone	3°
Gross Weight (incl. turbojets)	11,900 lb

respectively. The blade pitch on each individual rotor is given by

$$\theta_U = \theta_{0U} + \theta_{1CU}\cos(\psi_U + \Gamma) + \theta_{1SU}\sin(\psi_U + \Gamma)$$
$$\theta_L = \theta_{0L} + \theta_{1CL}\cos(\psi_L + \Gamma) + \theta_{1SL}\sin(\psi_L + \Gamma)$$

The rotor azimuth angle, ψ, increases in the direction of blade rotation. An azimuthal position of 0°is oriented towards the tail for both rotors. The XH-59 rotor is very stiff, so the flap response occurs much more quickly than on an articulated rotor. While θ_{1C} is used to produce lateral control for an articulated rotor, it is mostly the $\sin(\psi)$ terms that produce lateral control moments on the XH-59 rotor. Similarly, the $\cos(\psi)$ terms produce most of the longitudinal moments, while the $\sin(\psi)$ terms contribute very little. Γ is the phase offset, which serves to offset the azimuthal location in which the blade pitch is applied. Rather than keep the same nomenclature as an articulated rotor and set Γ close to -90°, the degrees of freedom are re-cast in terms of new variables which can also make the overall state of the rotor system easier to grasp. The new variables are the same as those described in Refs. 4 and 8 and are shown in Table 2.

Table 2. Rotor control variables

Collective	θ_0	$= \frac{1}{2}(\theta_{0U} + \theta_{0L})$
Differential collective	$\Delta\theta_0$	$= \frac{1}{2}(\theta_{0U} - \theta_{0L})$
Longitudinal	A_1	$= -\frac{1}{2}(\theta_{1CU} + \theta_{1CL})$
Differential longitudinal	A_1'	$= -\frac{1}{2}(\theta_{1CU} - \theta_{1CL})$
Lateral	B_1	$= -\frac{1}{2}(\theta_{1SU} - \theta_{1SL})$
Differential lateral	B_1'	$= -\frac{1}{2}(\theta_{1SU} + \theta_{1SL})$

With these new variables, the pitch on the upper and lower rotors is given by

$$\theta_U = \theta_0 + \Delta\theta_0 - (A_1 + A_1')\cos(\psi_U + \Gamma) - (B_1 + B_1')\sin(\psi_U + \Gamma)$$

$$\theta_L = \theta_0 - \Delta\theta_0 - (A_1 - A_1')\cos(\psi_L + \Gamma) + (B_1 - B_1')\sin(\psi_L + \Gamma)$$

The collective pitch, θ_0, now represents the average collective pitch of both rotors, while the differential collective, $\Delta\theta_0$, represents the difference in collective pitch of the upper and lower rotors from the average. The lateral pitch, B_1, represents pitch that is high on the left side of the helicopter and will cause a rightward roll moment. The longitudinal pitch, A_1, represents pitch that is high on the front of the helicopter and will cause a nose-up moment. A positive differential lateral pitch, B_1', represents increased pitch on the retreating sides of both rotors, and a negative value will increase pitch on both advancing sides. A positive value of differential longitudinal pitch, A_1', represents higher pitch on the front of the upper rotor, and on the back of the lower rotor. The differential longitudinal pitch is kept at zero or low values in the flight tests in Ref. 4 and is set to zero in all of the current simulations. There is no clear benefit to using differential longitudinal pitch; it would most likely lead to larger maximum hub moments.

The phase offset helps correct for the delayed response of the blades which, even though being stiff, have some flexibility. The effect of changing the rotor phase, Γ, could also be created by changing the cyclic and differential cyclic controls. Because the lateral cyclic pitch is generally small, the effect of using diferent values of Γ is the same as using different values of differential lateral pitch and longitudinal. Given that the current study already is investigating a range of differential lateral pitch, investigating different values of gamma would be redundant. The value used in the high speed flight testing (Refs. 4, 7) and current simulations is $\Gamma = 40°$.

Main Rotor Blades

The XH-59 has two 3-bladed rotors. Each blade is attached to the hub with a single pitch bearing. The blades have a 3°precone angle, and are linearly tapered. The aerodynamic sections of the blade begin at 20% span. The chord decreases from 20.7 in at 20% span to 11.5 in at the blade tips. The blade twist distribution and thickness to chord ratio are shown in Figure 1. RCAS models the rotor blades as elastic beams undergoing coupled flap bending, lag bending, and elastic torsion. The stiffness and mass properties are taken from Ref. 4. The blade was discretized using 10 equal length structural finite elements. The blades were modeled using several different airfoil sections, as indicated by Figure 1.

The airfoil sections used in the simulation and shown in Figure 1 are different from the actual airfoil sections on the XH-59; the actual airfoils used were the NACA 63(230)-224A, NACA 63(230)-213A and NACA 23012(64), as reported in Ref.5. The data for these sections was not available, so the similar NACA 0026, 63-218, and 23012, for which tables of the sectional lift, drag, and moment coefficients were available, were used. These are the same sections used to model the XH-59 in Ref. 8. While Ref. 8 applied the 3 aerodynamic tables to 3 distinct sections of the blade (inner, middle, and outer), the current model blends the data smoothly to represent the smooth variation of the the actual blade. Figure 1 shows that the blade sections taper in thickness to chord ratio from 26% to 12%. To re-create this effect, intermediate

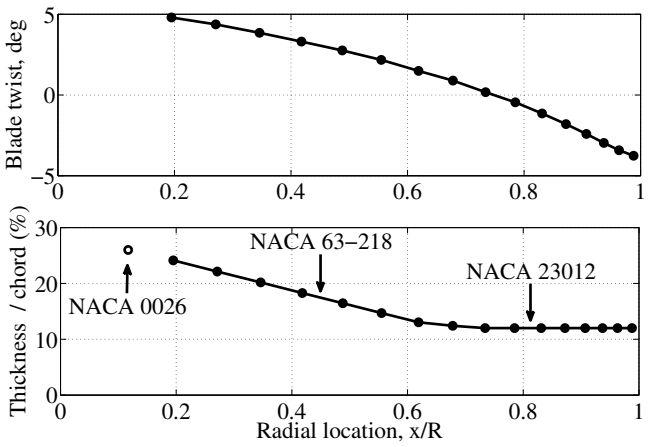

Fig. 1. Blade thickness and twist distribution

airfoil tables were created by interpolating between the airfoil section coefficients, based on airfoil thickness to chord ratio, between the 26% thick NACA 0026, the 18% thick NACA 63-218, and the 12% thick NACA 23012 (so each table matches the actual blade thickness where it is applied). There were 16 total aerodynamic sections used to model the blade, shown as the solid dots in Figure 1. The unfilled circle in Figure 1 marks the point where the NACA 0026 would be if it weren't within the root cutout.

Fuselage

The fuselage aerodynamic coefficients were obtained from the full-scale wind tunnel test data in Ref. 5. These data were used to construct fuselage lift and pitching moment coefficients that varied linearly with aircraft pitch attitude and a fuselage drag coefficient that varied quadratically with pitch. The fuselage aerodynamic coefficients included the effect of the hub, horizontal tail, and vertical stabilizers. The values used are given in Table 3. The fuselage lift and pitching moment are also shown in Figures 4 and 5. The aircraft gross weight (11,344 lbs) and locations of the center of gravity, rotors, and auxiliary jet engines are obtained from Ref. 4 and shown in Table 1. The propulsive force, representing the thrust of the two J60 engines, was applied as a point force at the engine attachment point.

The fuselage drag used by RCAS in Ref. 36 was larger than on the actual XH-59. The discrepency has since been corrected resulting in a smaller drag at the pitch attitudes being investigated. While the larger drag in Ref. 36 indicated that thrust required rose quickly as the aircraft pitch rose above (or below) nose level, the actual thrust required is significantly less at moderate pitch attitudes.

In Ref. 38 Passe et. al. showed that the rotor inflow produces significant down force on the fuselage and tail, as well as a pitch up moment, caused by the tail down force. Ref. 38 showed that for the X2, the rotor downwash created a downforce on the fuselage and tail amounting to about 19% of the vehicle weight. The same 19% of the XH-59's gross weight

Table 3. XH-59 fuselage and tail aerodynamic characteristics (α in radians)

L/Q (ft^2)	-3 + 305.3α
D/Q (ft^2)	13.9 + 158α^2
M/Q (ft^3)	30 - 2432α

(2262 lbs) was applied to represent the rotor download. Of the 19% total downforce in Ref. 38, about 7% was on the horizontal tail. This force caused a large pitch up moment. A pitch up moment (16,688 ft-lbs) corresponding to a tail download of 7% of the vehicle weight acting at a distance of 20 ft (the distance from the center of gravity to the horizontal tail) was also applied to the XH-59 model. The net download and nose up pitch moment are empirically modeled as point forces on the center of gravity of the aircraft. The downward force was added in the aircraft frame of reference so it changes direction as the aircraft pitches up. These forces are included in the fuselage lift and drag presented in this paper.

Rotor Inflow

The wake model from Ref. 36 has been improved by switching from the 8×8 state dynamic wake to a prescribed wake model. The wake uses 90 azimuthal segments per revolution, corresponding to 4 degree timesteps. The wake consists of a tip core which was extends for three revolutions behind the blades, 2 inboard wake sheets, also extenting three evolutions, and a near wake region which extends 30 °behind the blade. The size of the tip core was set to be 1/2 of the tip chord, while the root core and the cores of the near wake were set to 2 tip chords. The near wake includes both trailed and shed vortex elements, while the far wake only includes the trailed vorticies. The prescribed vortex wake was able to capture finer details of the blade vortex interactions while still keeping computation time relatively low.

Trim

In Ref. 36 vehicle trim was carried out by using six trim variables, collective, lateral cyclic, longitudinal cyclic, pedal (differential collective), pitch attitude, and roll attitude to drive the six forces and moments to zero. Other controls (Differential lateral pitch, Differential longitudinal pitch, propulsive thrust, and rotor RPM) were set to specified values. This method of trim has the shortcoming that, for a given level of propulsive thrust, it is possible to trim at more than one aircraft pitch. A new method of trim has been implemented where the six trim variables are collective, lateral cyclic, longitudinal cyclic, pedal (differential collective), roll attitude, and propulsive thrust, with the pitch attitude (as well as rotor RPM and differential lateral) being set to a specified value. By varying the pitch attitude, it is possible to investigate all possible pitch/thrust combinations. This method is similar to the trim procedures used by Refs. 21 and 23. To trim the helicopter, 90 time steps were used to find a periodic solution for the rotor inflow and blade deformations. Each trim variable is

perturbed to determine the Jacobian matrix and trim steps are taken until the residual forces are reduced to less than 50 lbs and the residual moments to less than 150 lbs. Once this state was achieved, the trimmed controls were used to run a new periodic solution using 360 time steps. The overall performance and rotor forces are changed only slightly by adding the additional time steps, but the periodic solution with 360 time steps gives better resolution for the blade loads.

ANALYSIS

The total vehicle power is the sum of the propulsive power, $P_{prop} = \frac{T_{prop} V_\infty}{\eta_p}$ and the rotor power. The propeller efficiency, η_p was chosen to be 0.9, which is in the range of what can be achieved by an efficient propeller, and also used by Johnson in Ref. 23.

$$P_{\text{total}} = P_{\text{rotor}} + \frac{T_{prop} V_\infty}{\eta_p}$$

If there is a large upwash through the rotor disk, as is the case when the rotor is tilted back, the rotor consumes less power. This power can even become negative, meaning that the rotor is extracting power. The current work assumes that the transmission is capable of providing the extracted rotor torque to help drive the propulsor. Current helicopters, such as the X2, are not configured to extract power from the main rotor, so they operate in a marginally powered state (Ref. 39). In addition to increasing the torque going to the propeller, the fact that the rotor is in a negative power state, allows the rotor to spin at lower speeds, whereas a free spinning rotor would speed up until the increased drag caused the rotor power become zero.

The rotor H-force, or rotor drag, is the overall drag produced by the rotor system. The rotor drag, F_x, is found by taking the sum of the blade forces in the x-direction (in the wind axes, towards the rear of the aircraft). The rotor effective lift to drag ratio, L/D_e, is computed using the rotor lift and drag forces along with the rotor power.

$$L/D_e = \frac{F_{z,w}}{(P_{rot}/V_\infty + F_{x,w})}$$

Another important parameter is the rotor lift-offset, which can be thought of as the lateral location of the center of lift of each rotor. It is calculated as

$$LOS = \frac{\Delta M_x}{TR}$$

where ΔM_x is the difference between the lateral moments between the upper and lower rotor, T is the combined thrust of the two rotors, and R is the rotor radius.

VALIDATION

The RCAS simulation model was validated against several pieces of test data. Figure 2 shows the rotor effective lift to drag ratio compared against flight test data and a CAMRAD simulation from Ref. 23.

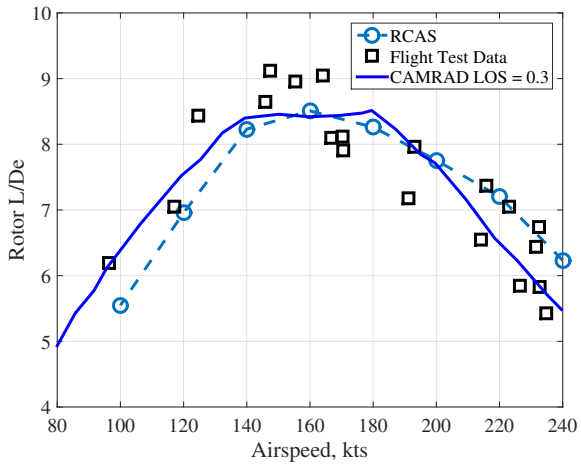

Fig. 2. Rotor Lift to drag ratio

In Figure 1 the pitch attitude is reduced from 9 °nose up to 0°(nose level) with increasing speed, similar to the curve shown in Ref. 7. The rotor speed is held constant at 97% Nr and the differential lateral pitch is adjusted to keep the lift offset at approximately 0.3.

The blade flatwise root bending moments are shown in Figure 3 along with flight test data. The comparison shows a trend for loads to decrease with increasing differential lateral pitch. The differential lateral pitch in the flight test data was given as a function of percent in Ref. 4 and converted to degrees using the control range given in Ref. 3.

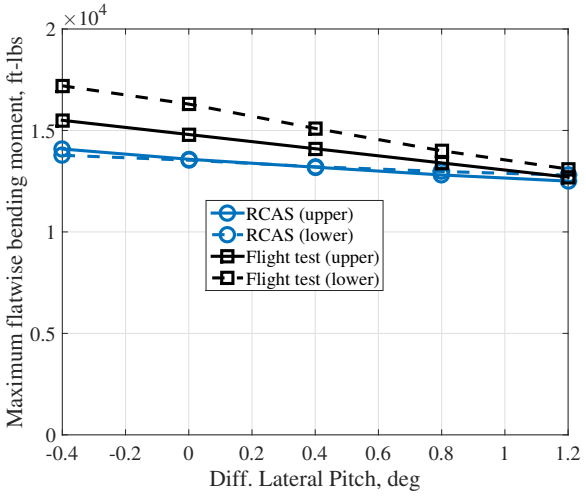

Fig. 3. Flatwise bending moment at 10% radius, 1/2 peak to peak, 4 °pitch attitue, 210 kt

RESULTS AND DISCUSSION

A variety of test cases were run at 6,000 ft altitude, 95°F, and a flight speed of 230 kts, which corresponds to the current target

for the JMR TD requirement.

Vehicle Forces and Trim

As the aircraft pitch attitude increases, the horizontal tail produces a greater vertical force and lessens the total lift needed by the main rotor. Figure 4 shows the rotor and fuselage lift as a function of vehicle pitch attitude. This figure is independent of rotor speed or differential lateral pitch. The effects due to the rotor downwash are included in the fuselage forces shown in Figure 4, as well as the moments in Figure 5.

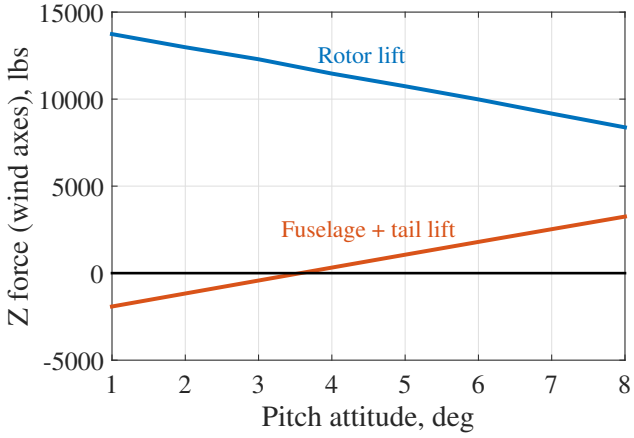

Fig. 4. Vertical forces vs. aircraft pitch attitude, 230 kt

Considering Figure 4, as the vehicle tilts back from 3°to 7°, the rotor thrust decreases by 26.7%. It will be shown that this decreased thrust will lead to a decrease in power and increase in rotor L/D_e due to the fact that the lifting function of the rotor is being transferred to the horizontal tail.

Figure 5 shows the fuselage and rotor pitching moments as a function of aircraft pitch. The horizontal tail is mounted at a slightly negative incidence. This results in a nose up pitching moment at low aircraft pitch and a nose down (negative) pitching moment at higher aircraft pitch. The rotor will produce a counter acting moment in order to trim the aircraft, which is a nose down moment below about 4°pitch attitude and a nose up moment at higher pitch attitudes. The current simulation uses a fixed horizontal lifting surface; if the horizontal tail were to be controllable via incidence change or elevator, which is common in other helicopters, the rotor would not need to produce any pitching moments and greater variety of trim states would be allowed.

The auxiliary propulsor and fuselage drag can contribute to the vehicle pitching moments, causing the rotor moment to vary slightly at a given aircraft pitch attitude, but these variations are small compared to the rotor and tail moments.

Total Power

The aircraft was trimmed with rotor speeds ranging from 90% Nr (310.3 RPM) to 40% Nr (137.9 RPM), pitch attitudes ranging from 1°to 8°in 1°increments, and differential lateral pitch

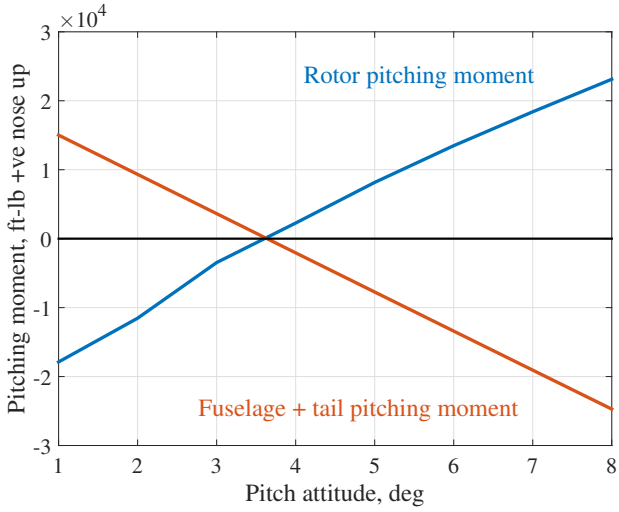

Fig. 5. Pitching moments vs. aircraft pitch attitude, 230 kt

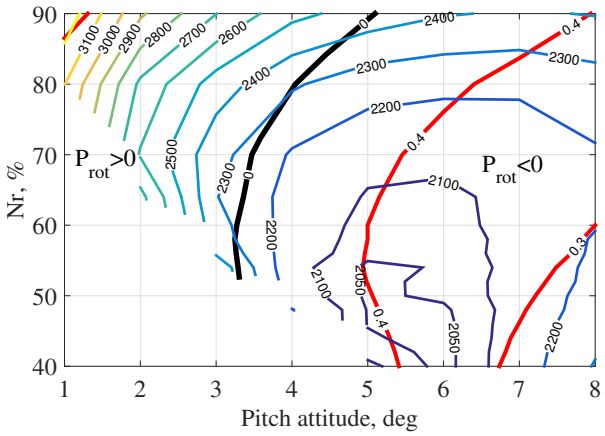

Fig. 6. Total Power, HP, differential lateral pitch = -9°

settings from -9°to 3°. Figures 6, 7, 8, 9, and 10 show the total vehicle power as a function of aircraft pitch and rotor speed, with increasing differential lateral pitch. Also shown on the figures are contours indicating zero rotor power conditions (black line), and different levels of lift offset (red lines). The rotor power is positive to the left of the P_{rot} = 0 curve. As the aircraft pitch increases above about 3°, the rotor power reaches zero and then becomes negative to the right of the curve. At low aircraft pitch and rotor speeds, the rotor will be incapable of trim. At pitch attitudes of 4 °and below the rotor speed was decreased as low as it was possible to trim.

The conditions at which the lowest power occurred for different values of differential lateral pitch were all at significantly slowed rotor speeds (40–65% Nr) and high aircraft pitch attitude (6–7°). The power in this region was very close (within about 20 HP) for all the differential lateral pitch settings. It can be seen that the overall minimum power trim state is well into the negative rotor power region. In addition to this state, we also consider the minimum total power for a

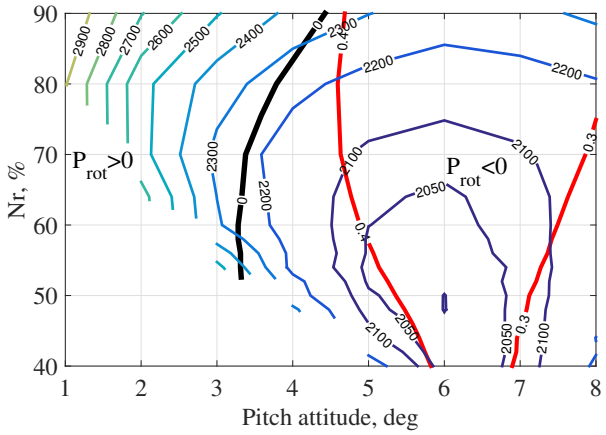

Fig. 7. Total Power, HP, differential lateral pitch = -6°

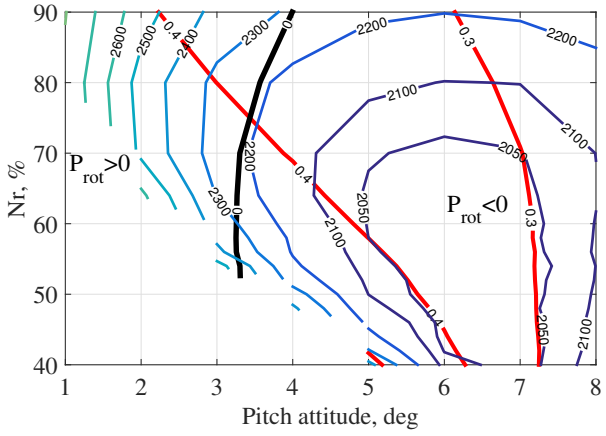

Fig. 8. Total Power, HP, differential lateral pitch = -3°

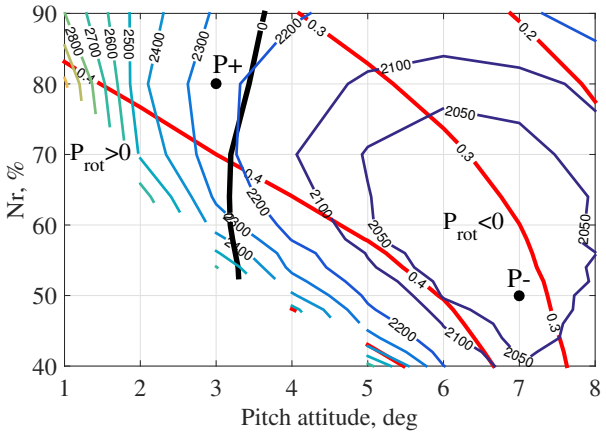

Fig. 9. Total Power, HP, differential lateral pitch = 0°

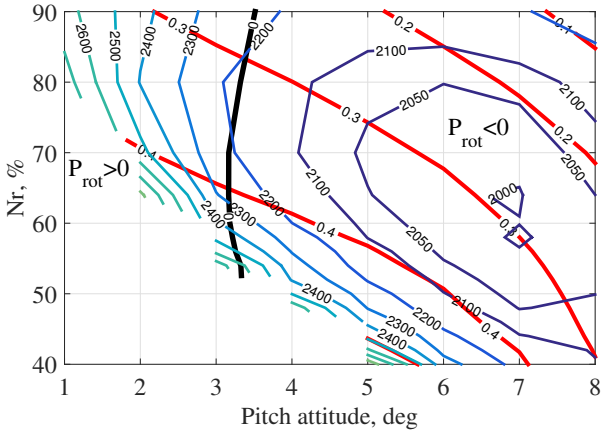

Fig. 10. Total Power, HP, differential lateral pitch = 3°

marginally powered rotor, which will lie close to the $P_{rot} = 0$ curve. Two trim states exemplifying the marginally powered state and the negative rotor power state have been marked P+ and P- on Figure 9. The present work will compare these two cases extensively. A diagram comparing major forces and moments for these two trim states is shown in Figure 11. These and other details of the trim states are listed in Table 4. This data shows that using the main rotor to drive the propulsor results in a 9.6% reduction in total power by moving from the marginally powered rotor state to the negative rotor power state.

Lift offset

The contours of lift offset in Figures 6–10 show that the lift offset decreases as the pitch of the vehicle increases. The lift offset also depends on the rotor speed and differential lateral pitch. This relationship is illustrated in Figure 12. The figure shows that at high rotor speeds increasing the differential lateral pitch (reducing blade pitch on the advancing sides) decreases the lift offset, but as the rotor speed is lowered, lift offset begins to increase with differential lateral pitch.

Rotor L/D_e

Figure 13 shows the rotor lift to drag ratio as a function of pitch attitude and rotor speed with a differential lateral pitch of 0°. The rotor lift to drag ratio follows similar trends to the total power as it also takes into account both rotor power and the drag produced by the rotor. The best performance is at high pitch attitudes and significantly slowed rotor speeds where L/D_e can reach as high as 18. There was only a slight variation in the maximum L/D_e (from 18 to 17) over the range of differential lateral pitch settings. Recalling the formula for lift offset

$$L/D_e = \frac{F_{z,w}}{(P_{rot}/V_\infty + F_{x,w})}$$

a negative rotor power will decrease the denominator and increase L/D_e. Figure 13 also shows that for a marginally powered rotor the maximum L/D_e is between 12 and 13, indicated by the states along the $P_{rot} = 0$ line. L/D_e increases by 30% from the P+ to P- trim states.

Bagai (Ref. 10) showed that at high speeds (230 kts and above) rotor L/D_e increased with pitch up to about 6°, at

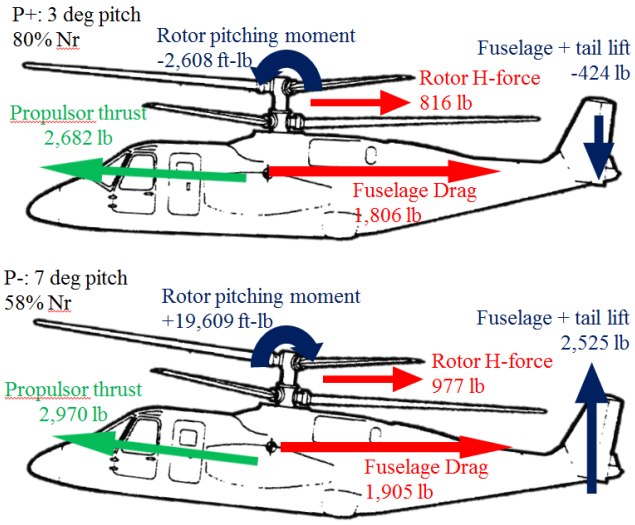

Fig. 11. Comparison of trim forces and moments

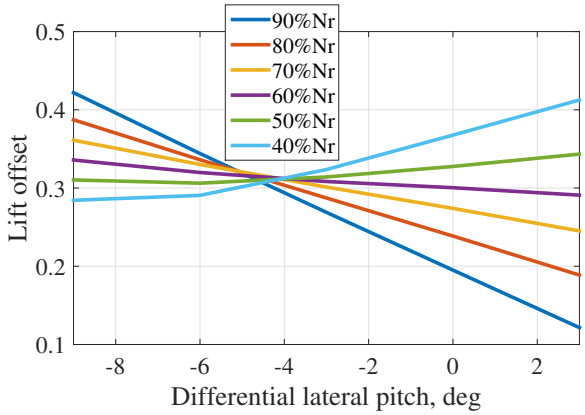

Fig. 12. Lift offset, aircraft pitch = 7°

which point it reached its maximum and began to decrease. The current results show the same trend. Current helicopters have achieved a maximum L/D_e as high as 10 (for the X2 (Ref. 10)) to 12 (for the Cartercopter (Ref. 40)). The current results highlight the fact that current helicopters are limited in maximum L/D_e because they cannot extract power from the rotor, and enabling these states can lead to significant improvements.

Table 4. Comparison of minimum power in marginally powered and power extraction states

	P+	P-
Rotor speed (% of Nr)	80%	50%
Advance Ratio	0.75	1.19
Advancing tip Mach no.	0.78	0.62
Lift-offset	0.36	0.33
Collective pitch (θ_{75})	9.2°	3.9°
Longitudinal pitch	-10.3°	-5.7°
Differential lateral pitch	0°	0°
Aircraft pitch attitude	3°	7°
TPP angle of attack (average)	2.6°	7.9°
Lon. flapping (average)	0.4°	-0.9°
Lateral flapping (average)	2.3°	1.99°
Rotor Thrust (lbs)	11,471	8,427
Rotor H-force (lbs)	816	977
Propulsor Thrust (lbs)	2,682	2,970
Fuselage drag (lbs)	1,805	1,905
Rotor Pitching moment (ft-lb)	-2,608	19,609
Total Power (hp)	2,228	2,014
Propulsor Power (hp)	2,104	2,329
Main Rotor power (hp)	124.8	-314.7
Rotor L/D_e	12.4	17.7
Root chordwise shear (lb)	406	222
Root normal shear (lb)	3,582	2,295
Max root flatwise bending (ft-lb)	26,644	21,695
Root chordwise bending (ft-lb)	3,568	6,079
Root torsional bending (ft-lb)	173	153
3P hub vertical force (lbs)	679	465
3P hub H-force (lbs)	841	872
3P hub lateral force (lbs)	156	24
3P hub pitch moment (lb-ft)	15,671	2,237
3P hub roll moment (lb-ft)	1,270	2,381

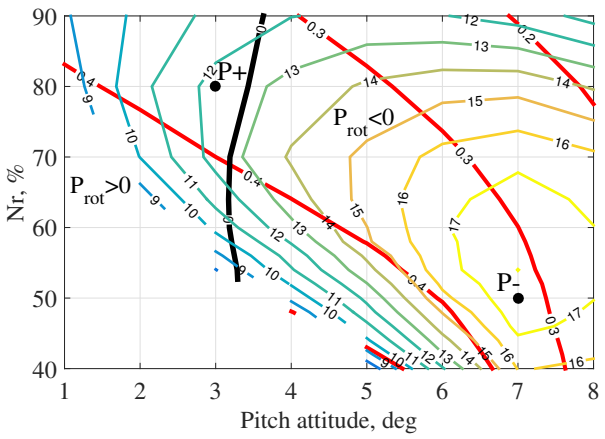

Fig. 13. Rotor effective lift to drag ratio, differential lateral pitch = 0°

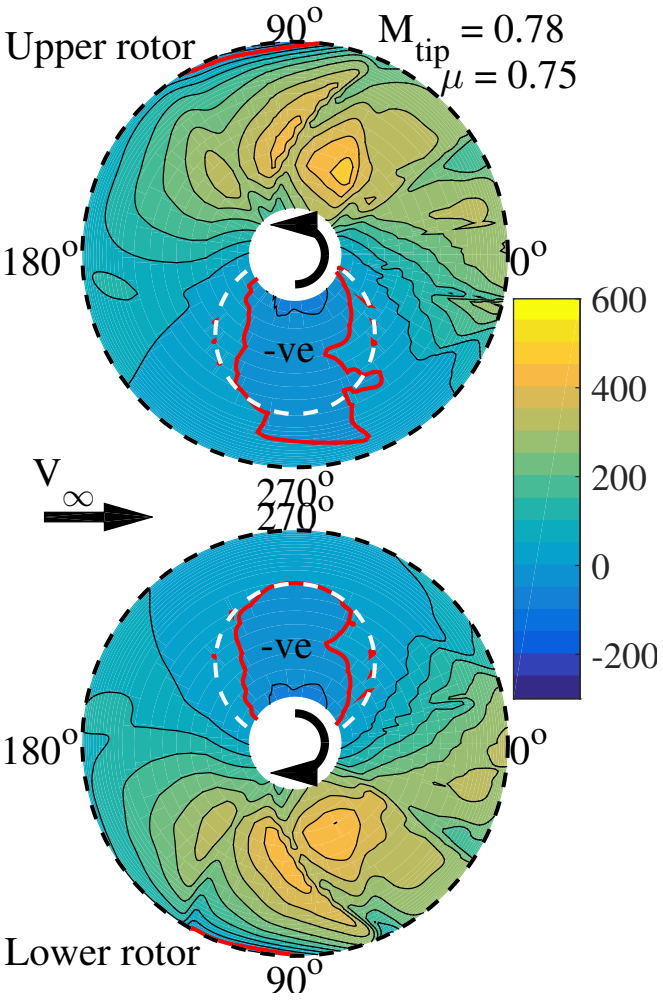

Fig. 14. Blade lift per unit span (lbs/ft), 80%Nr, 3°aircraft pitch, differential lateral pitch = 0°

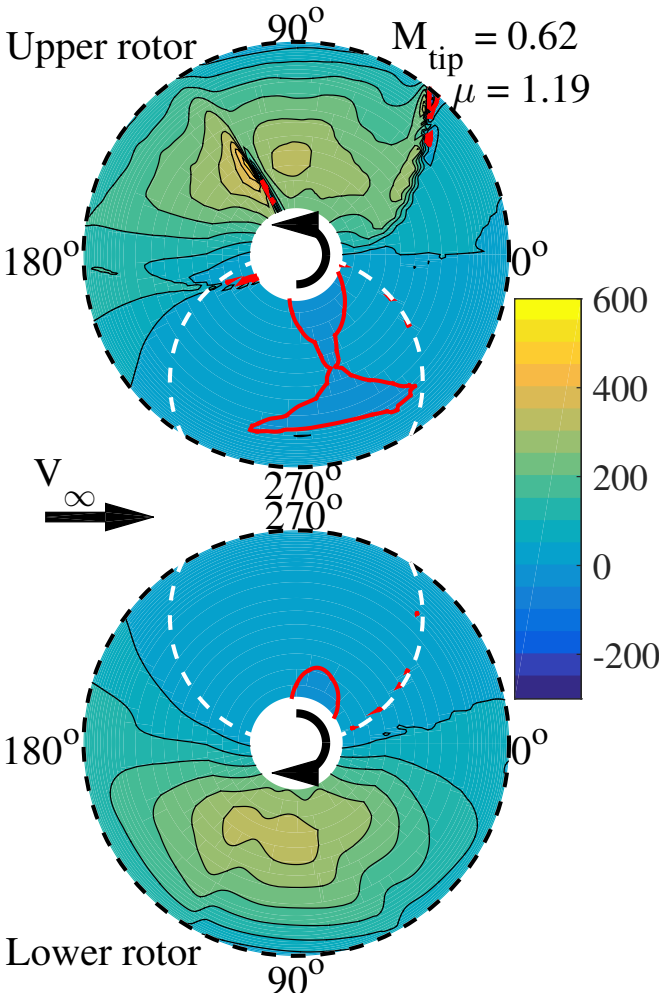

Fig. 15. Blade lift per unit span (lbs/ft), 50%Nr, 7°aircraft pitch, differential lateral pitch = 0°

Rotor Aerodynamics

The two trim states discussed earlier, P+ and P-, are further examined by looking at the distributions of blade lift and drag, shown in Figures 14, 16, 15, and 17. Also shown on the figures is a white dotted line representing the boundary of the reverse flow region. Regions of positive and negative lift or drag have been marked and the boundary between the positive and negative regions is indicated by a red line.

Comparing the lift in Figures 14 and 15, blade vortex interactions are visible on the advancing side for both conditions. When the rotor is at a low pitch, as in Figure 14, the blades can pass through the tip vortex of the preceding blades. This is seen in Figure 14 on the advancing sides of both the upper and lower rotors. The strongest interaction can be seen as a discontinuity in the blade lift near 90°azimuth. Slightly weaker interactions are seen near the rear of the disk.

When the aircraft is at high pitch attitude as in Figure 15, there is a large upwash through the rotor disk. This upwash helps to carry the tip vorticies up above the disk. In certain conditions the tip vorticies from the lower rotor can flow through the upper rotor. Instances of this are seen in Figure 15. There are 2 blade vortex interactions on the advancing side of the upper rotor, but none on the lower rotor.

While nearly all of the reverse flow region produces negative in Figure 14, the additional upwash in Figure 15 serves to make much of the reverse flow region produce positive lift. The advancing blade tips also show the same effect. In Figure 14 the rotor is producing a nose down pitching moment, as indicated by the relatively larger lift on the rear of the disk compared to the front. Figure 15 shows the opposite, with more lift produced at the front of the disk.

With regards to the blade drag, the upwash through the rotor disk in Figures 16 and 17 leads to negative induced angles of attack and large regions of negative drag which provide an accelerating force to the blades. As the blade enters the reverse flow region, there are regions of positive lift, which, when coupled with the upwash, lead to positive drag. In Figure 16, the regions of positive and negative drag are approximately equal, leading to a marginally powered state. In con-

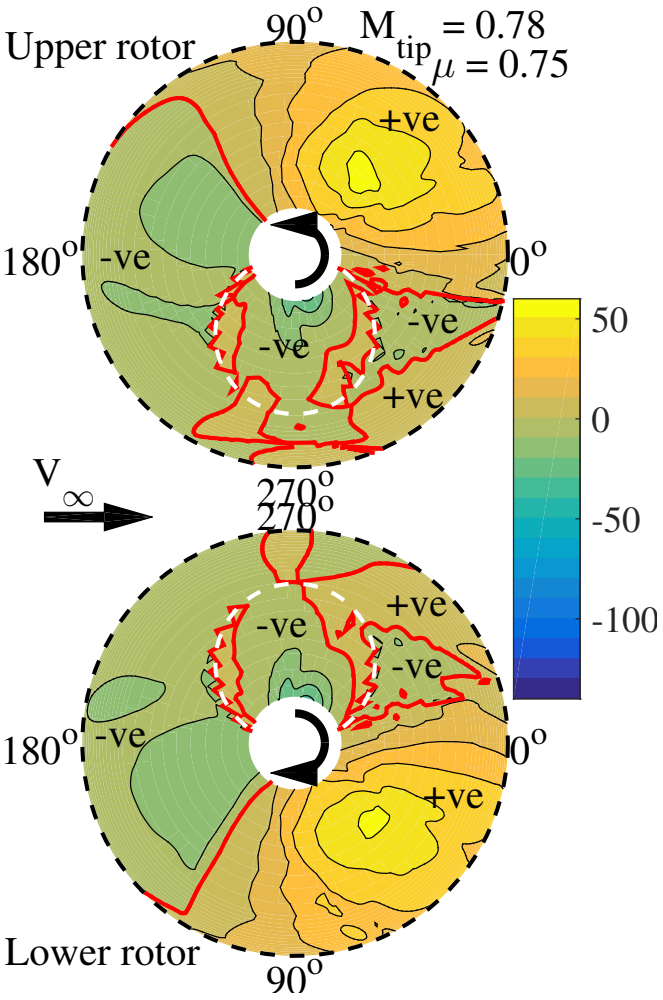

Fig. 16. Blade drag per unit span (lbs/ft), 80%Nr, 3°aircraft pitch, differential lateral pitch = 0°

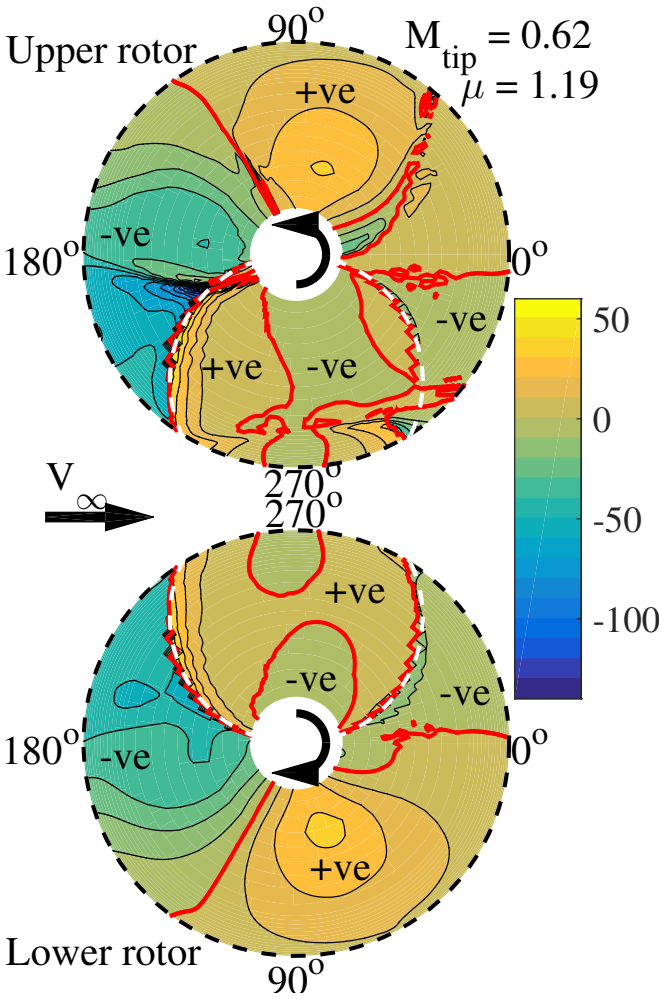

Fig. 17. Blade drag per unit span (lbs/ft), 50%Nr, 7°aircraft pitch, differential lateral pitch = 0°

trast, Figure 17 has lower drag on the advancing side, and greater amounts of negative drag, leading to an overall negative torque. The greater drag on the advancing side of Figure 16 is due to the larger dynamic pressure on the faster spinning blades. The negative drag in the reverse flow region of Figure 16 is also greater than in 17. This is due to the high pitch of the blade sections near the root.

The blade pitch at 75% span is shown in Figure 18. The pitch at the root is 4°greater than the pitch at 75% span. For the P+ state, the root pitch at $\psi = 270^o$ is 20°and the angle of attack is 11.9°(from the trailing edge). For the P- state, there is only 11.3°root pitch and 1.8°angle of attack from the trailing edge. It is because of the the high blade pitch and high drag in this region that the designers of the X2 used double ended airfoils and a shortened chord.

Blade Loads

Blade loads are important to consider when assessing different flight states of the vehicle. For an articulated rotor the blade loads could be maximum at any point along the blade, depending on flight conditions and how the blades deform. For a hingeless rotor, such as the XH-59 or the X2, the largest blade loads will most likely occur at the root near the advancing side.

Figure 19 shows the blade flatwise and lag bending moments for the two trim states compared in Table 4. The upper rotor loads (solid line) are very similar to the lower rotor loads (dashed line). The maximum flatwise bending loads, marked by a circle for the upper rotor and a square for the lower rotor, occur near 90°azimuth due to the high lift on the advancing side. The maximum values of flatwise bending are also reported in Table 4. There is a discernible difference between the upper and lower rotor for the P- flatwise bending loads over much of the advancing side. The upper rotor loads show sharp variations indicative of the blade vortex interaction seen in Figure 15 which are absent on the lower rotor.

The blade lift and drag distributions in Figures 14–17 are reflected in the root moments in Figure 19. The more even distribution of lift for the 7°pitch state results in a more even distribution of flatwise moment around the azimuth. The difference in overall pitching moment generated by the rotor is

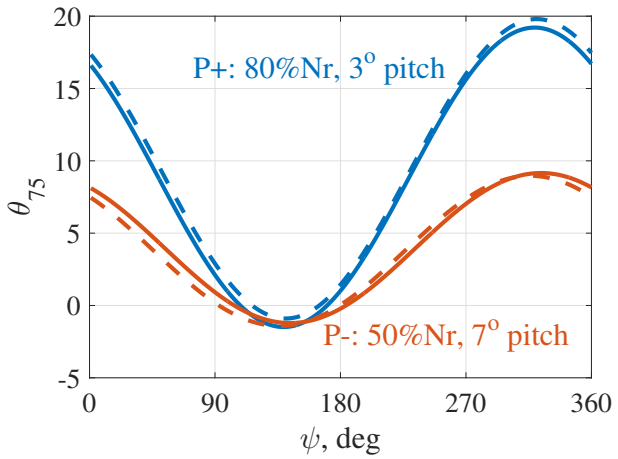

Fig. 18. Blade pitch at 75%span, differential lateral pitch = 3°

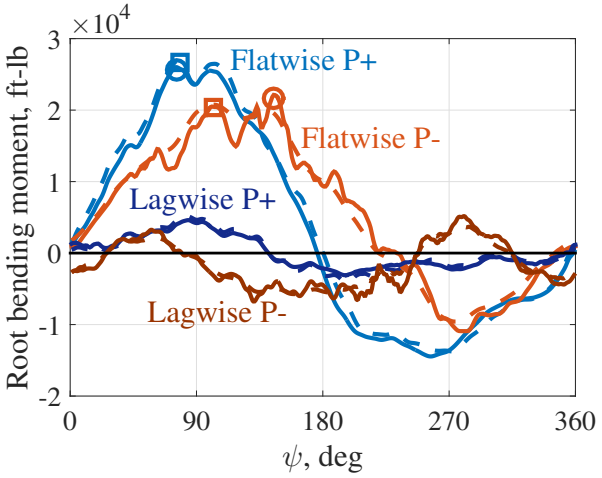

Fig. 19. Blade root bending moments (ft-lb) at 10% radius, differential lateral pitch = 3°

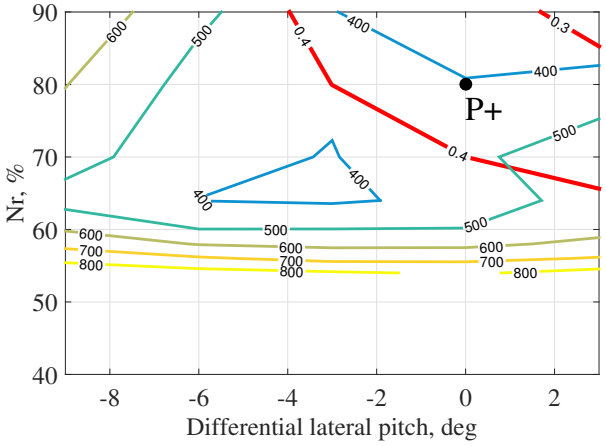

Fig. 20. Blade chordwise shear force, lbs (1/2 peak to peak) at 10% radius, aircraft pitch = 3°

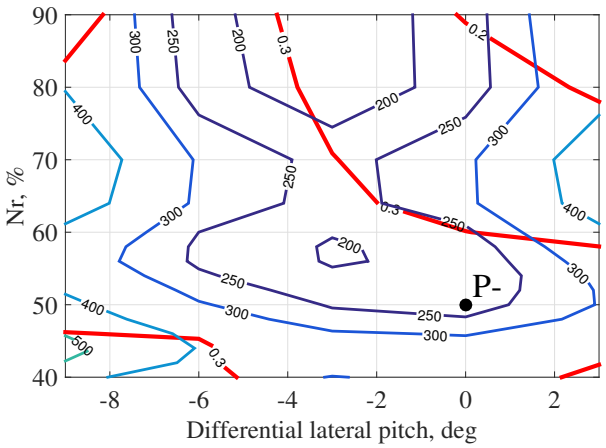

Fig. 21. Blade chordwise shear force, lbs (1/2 peak to peak) at 10% radius, aircraft pitch = 7°

highlighted by the flatwise bending near 180°azimuth, which is significantly higher for the 7°pitch state. The bending moment becomes negative near 270°for both cases due to the negative lift generated in the reverse flow region.

Figure 19 shows that the lag moment for the P+ pitch state is positive (contributing to rotor power required) over most of the advancing side but negative on the retreating side due to the negative blade drag in this region. The integrated lag moment is only slightly above zero, indicating the small amount of power required. The P- state has much larger regions of negative lag moment near 0°and 180°azimuth, which put the rotor into a negative power state.

Figure 20 shows the unsteady chordwise shear forces (1/2 peak to peak values) for an aircraft pitch of 3°over a range of differential lateral pitch and rotor speeds. The 1/2 peak to peak value is half of the difference between the maximum and minimum load and is a common metric used with unsteady blade loads. Like the plots of power and L/D_e, the lift offset is shown in red. The line for P_{rot} = 0 is not visible on this figure because the rotor power is always positive at 3 deg aircraft pitch. The P+ trim state at 80%Nr and 0 deg differential lateral pitch is marked on the figure. Figure 20 shows that the chordwise shear will increase sharply below rotor speeds of 60%Nr. At the P+ trim state the rotor speed is well above this and the 1/2 peak to peak chordwise shear is 406 lbs.

Figure 21 shows the chordwise shear for an aircraft pitch of 7 deg. The rotor power is negative for all of the states in this figure. At the P- trim state, the 1/2 peak to peak shear loads are lower than the P+ state, at only 222 lbs. These values are also reported in Table 4.

The blade normal shears (1/2 peak to peak vlaues) at aircraft pitches of 3°and 7°are shown in Figures 22 and 23. Comparing the two figures, the normal shear loads are smaller at 7°aircraft pitch.

Figures 24 and 25 show the maximum blade root flatwise bending moments for 3°and 7°aircraft pitch. For nearly all of

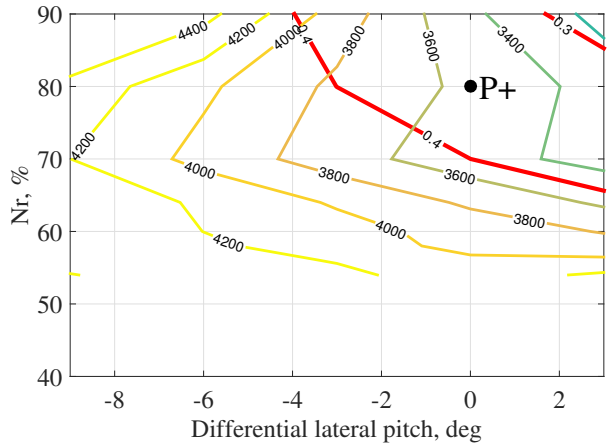

Fig. 22. Blade normal shear force, lbs (1/2 peak to peak) at 10% radius, aircraft pitch = 3°

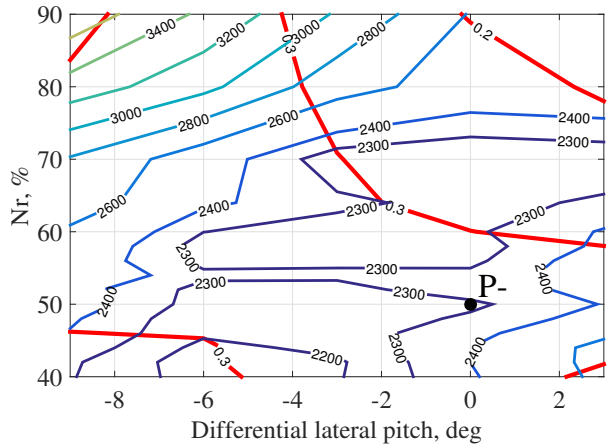

Fig. 23. Blade normal shear force, lbs (1/2 peak to peak) at 10% radius, aircraft pitch = 7°

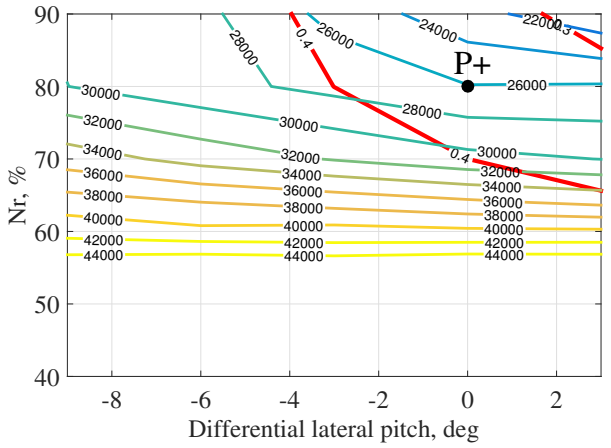

Fig. 24. Blade maximum flatwise bending moment (ft-lb) at 10% radius, aircraft pitch = 3°

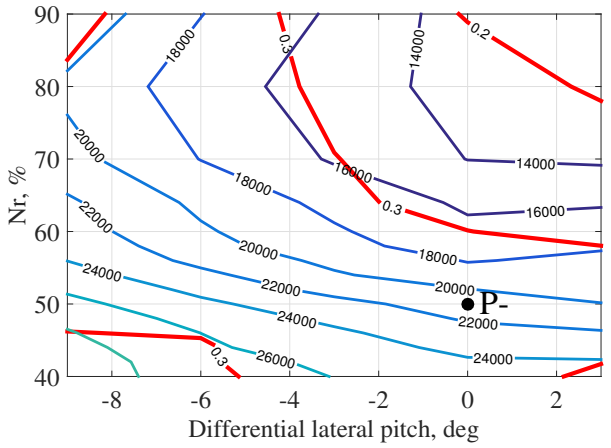

Fig. 25. Blade maximum flatwise bending moment (ft-lb) at 10% radius, aircraft pitch = 7°

the cases shown in Figures 24 and 25 the maximum flatwise bending moment occured near $\psi = 90°$, as in Figure 19. For a few cases, the maximum flatwise bending was negative and occurred close to the retreating side.

For both 3°and 7°aircraft pitch, the maximum flatwise bending loads increase with decreasing rotor speed. The difference in loads between Figures 24 and 25 also shows that increased aircraft pitch will also decrease the maximum blade loads. A combination of increasing pitch and decreasing rotor speed can keep the maximum bending relatively unchanged. The endurance limit root moment for the XH-59 blade is 16,500 ft-lb (Ref. 4). Because both the P+ and P- trim states exceed this limit, in practice, the aircraft pitch or rotor speed would need to be increased to keep blade loads within limits.

Overall, the blade loads at the P- trim state are either similar in magnitude or smaller than the corresponding loads at the P+ trim state. These loads are summarized in Table 4.

Hub vibrations

The XH59 simulation model incorporates 3 bladed rotors, and therefore the dominant vibratory loads are at a frequency of 3/rev. On a coaxial helicopter, the vibratory forces and moments are transmitted through each rotor shaft into the gearbox where the loads from the two rotors combine and are transmitted to the rest of the airframe. In the current work, the loads are analyzed by simply adding the loads from the hub of each rotor. While the loads at a specific point on the fuselage or gearbox will be different, these combined loads are representative of the overall forces and moments generated by the rotor system. The sin and cos components of each rotor force are added separately so that the resulting force has the proper magnitude and phase. The vibratory force in the longitudinal (x) direction is

$$F_x = \sqrt{(F_{x,\cos,U} + F_{x,\cos,L})^2 + (F_{x,\sin,U} + F_{x,\sin,L})^2}$$

This formula is valid for any harmonic so it applies to steady as well as vibratory loads. The formulas for the y and z forces and the x and y moments are similar.

Coaxial helicopters have unique vibration characteristics; as described in Refs. 4, 9 and 11, depending on the blade crossover angle, certain components of the rotor forces and moments will cancel out at the hub. For example, the current simulations have a 0°crossover angle meaning that blades of the upper and lower rotor cross over one another at 0°azimuth, or directly over the tail. In this configuration, the lateral vibratory forces, which are largely due to blade drag near 0°and 180 °azimuth, are in opposite directions for the upper and lower rotor at a given time, or in other words $F_{y,cos,u}$ is similar in magnitude, but opposite in sign to $F_{y,cos,l}$. When these forces are combined, the result is near zero and the vibrations felt at the hub are relatively low. In contrast, the longitudinal vibratory forces, which are due to chordwise blade drag near 90°and 270 °azimuth and radial drag near 0°and 180°, are in the same direction for the upper and lower rotor at a given time (blades of both the upper and lower rotor are at 90°azimuth simultaneously), which leads the longitudinal 3/rev vibratory force to be much larger in comparison. Similarly, the vertical vibratory forces add, the roll moments cancel, and the pitching moments add. By changing the blade crossover angle, these trends could be changed (if the blades crossed at 90°, then the roll moments would add and the pitch moments would cancel). Ref. 4 reported that the 0°crossover angle flight tests had smaller vibrations. All of the current simulations use a 0°crossover angle.

The 3/rev vertical hub vibratory force is shown over a range of rotor speeds and differential lateral pitch in Figure 26 and 27. The hub vertical force at the P- trim state is smaller than the P+ state.

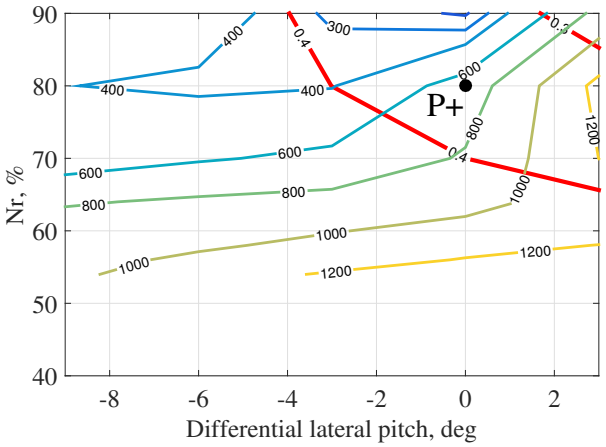

Fig. 26. Hub 3/rev vibratory vertical force (lb), aircraft pitch = 3°

The 3/rev hub vibratory H-force is shown in Figures 28 and 29. In previous work (Ref. 36) it was shown that hub vibrations became very high as rotor speed approached about

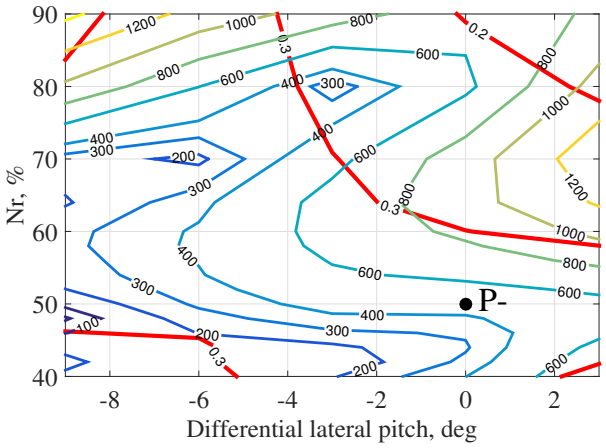

Fig. 27. Hub 3/rev vibratory vertical force (lb), aircraft pitch = 7°

65%Nr because the 2/rev excitation frequency approached the blade natural frequency. The current plots also show regions of large vibratory force near 65%Nr, but a rotor speed of 50%Nr stays well below these regions. The 3P vibratory H-force for the P- trim state is slightly larger (4%) than the P+ state.

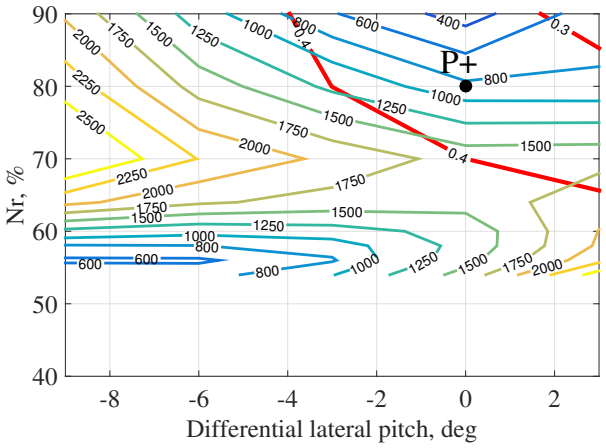

Fig. 28. 3/rev vibratory H-force (lb), aircraft pitch = 3°

The 3/rev hub pitching moments are shown in Figures 30 and 31. The 3P pitching moments are generally much larger than the roll moments due to inter-rotor cancellation. At 7°aircraft pitch the pitching moment vibrations reach a minimum near 0°differential lateral, seen in Figure 31. This region does not persist at different values of diferential lateral pitch, as shown in Figure 30.

The 3/rev pitching moments are a result of the 2/rev and 4/rev components of the blade root flapping and torsion moments. Figure 32 shows the contributions from the 2/rev and 4/rev blade root moments. At the P+ trim state, the contributions from the 2/rev blade loads are much larger than the 4/rev

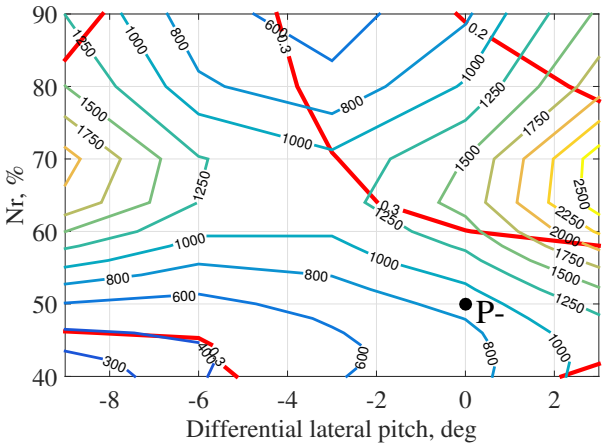

Fig. 29. 3/rev vibratory H-force (lb), aircraft pitch = 7°

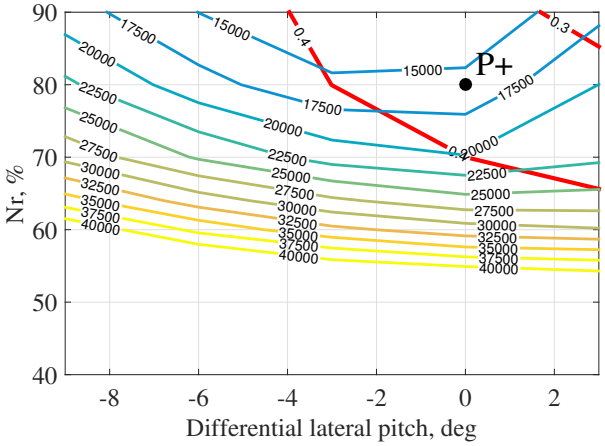

Fig. 30. Hub 3/rev vibratory pitch moment (ft-lb), aircraft pitch =3°

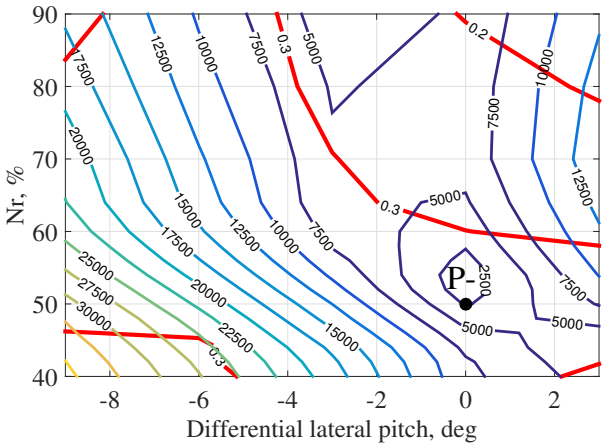

Fig. 31. Hub 3/rev vibratory pitch moment (ft-lb), aircraft pitch =7°

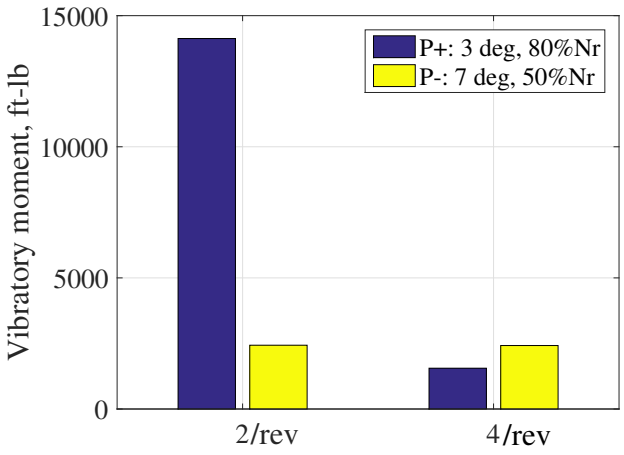

Fig. 32. Hub 3/rev vibratory pitch moment components (ft-lb), differential lateral pitch = 0°

blade loads. At the P- trim state, the 2/rev blade pitch moments are greatly reduced, which explains why the vibrations are significantly lower. Generally there is a large 2/rev component in the blade loads, which manifests in the 3/rev hub vibrations. It is for this reason that modern high speed helicopters, such as the X2, have switched to 4 bladed designs.

Overall, the hub vibratory forces and moments at the marginally powered rotor trim state are significantly larger than at the negative rotor power state. This is important as it shows that the benefits in performance achieved by moving to this state are not plagued by excessive vibrations.

CONCLUSIONS

1. The benefits of allowing the rotor to operate in a negative power state are twofold; the torque load on the rotor allows it to operate at a lower speed ($< 60\%$ of Nominal), reducing rotor power, and that power can be used for propulsion, lessening the total power required by up to 9.6% from the marginally powered state.

2. A horizontal tail can significantly reduce the necessary thrust of the rotor by producing lift. This reduction in rotor thrust can lead to improvements in rotor L/D_e. If the tail is producing a large lifting force, the rotor must produce a nose up pitching moment to balance the helicopter; therefore the amount of lift that is produced by the tail is limited by the moment that the rotor can produce.

3. By simultaneously pitching the aircraft and rotor aft to 6 or 7°and decreasing rotor speed to approximately 50%Nr, significant benefits in rotor performance can be achieved while keeping blade loads and vibratory forces and moments similar or decreased from the optimal marginally powered rotor state.

4. The dominant source of vibrations on a 3 bladed rotor is from 2/rev blade loads. Minimizing these 2/rev loads by flying at at large pitch attitudes (6 to 7 degrees) and low rotor speeds (50%Nr) can lead to reduction in vibratory forces and moments.

Author contact: George Jacobellis, gjacobellis@gmail.com

REFERENCES

[1]Hirschberg, M., "JMR Technology Demonstration Update: The Road to Future Vertical Lift," *Vertiflite*, January/February 2016, pp. 23.

[2]Leishman, J. G., *The Helicopter - Thinking Forward, Looking Back*, College Park Press, College Park, MD, 2007.

[3]Ruddell, A. J., "Advancing Blade Concept (ABC™) Development," *Journal of the American Helicopter Society*, January 1977.

[4]Ruddell, A., "Advancing Blade Concept (ABC) Technology Demonstrator," Technical report, U. S. Army Research and Technology Labotratories (AVRADCOM), USAVRADCOM-TR-81-D-5, Apr 1981.

[5]Felker, Fort F. III, "Performance and Loads Data from a Wind Tunnel Test of a Full-Scale, Coaxial, Hingless Rotor Helicopter," , (NASA TM 81329), October 1981.

[6]Phelps, A. E. and Mineck, R. E., "Aerodynamic Characteristics of a Counter-Rotating, Coaxial, Hingeless Rotor Helicopter Model With Auxiliary Propulsion," Technical report, National Aeronautics and Space Administration, NASA Technical Memorandum 78705, 1978.

[7]Ruddell, A. J., "XH-59A ABC Technology Demonstrator Altitude Expansion and Operational Tests," Technical Report USAAVRADCOM-TR-81-D-35, U. S. Army Research and Technology Laboratories (AVRADCOM), Dec 1981.

[8]Pleasants, W. A., "A Rotor Technology Assessment of the Advancing Blade Concept," Technical report, National Aeronautics and Space Administration, NASA Technical Memorandum 84298, 1983.

[9]O'Leary, J. and Miao, W., "Design of Higher Harmonic Control for The ABC," *Journal of the American Helicopter Society*, Vol. 27, (1), January 1982, pp. 52–57.

[10]Bagai, A., "Aerodynamic Design of the X2 Technology Demonstrator™ Main Rotor Blade," 64th Annual Forum of the American Helicopter Society, Montreal, Canada, April 2008.

[11]Blackwell, R. and Millot, T., "Dynamics Design Characteristics of the Sikorsky X2 Technology™ Demonstrator Aircraft," American Helicopter Society 64th Annual Forum, May 2008.

[12]Walsh, D., Weiner, S., Arifian, K., Bagai, A., Lawrence, T., and Blackwell, R., "Development Testing of the Sikorsky X2 Technology™ Demonstrator," 65th Annual Forum of the American Helicopter Society International, Grapevine,TX, 2009.

[13]Walsh, D., Wiener, S., Arifian, K., Lawrence, T., Wilson, M., Millott, T., and Blackwell, R., "High Airspeed Testing of the Sikorsky X2 Technology™ Demonstrator," 67th Annual Forum of the American Helicopter Society International, Virginia Beach, VA, 2011.

[14]Syal, M. and Lieshman, J. G., "Aerodynamic Optimization Study of a Coaxial Rotor in Hovering flight," *Journal of the American Helicopter Society*, Vol. 57, (042003), 2012.
doi: 10.4050/JAHS.57.042003

[15]Lieshman, J. G. and Ananthan, S., "An Optimum Coaxial Rotor System for Axial Flight," *Journal of the American Helicopter Society*, Aug 2008, pp. 367–381.

[16]Hersey, S., Sridharan, A., and Celi, R., "Multiobjective Performance Optimization of a Coaxial Compound Rotorcraft Configuration," Fifth Decennial AHS Aeromechanics Specialists Conference, San Francisco, CA, Jan 2014.

[17]Rand, O. and Khromov, V., "Compound Helicopter: Insight and Optimization," American Helicopter Society 69th Annual Forum, Phoenix, Arizona, May 2013.

[18]Schmaus, J. and Chopra, I., "Aeromechanics for a High Advance Ratio Coaxial Helicopter," AHS 71st Annual Forum, 2015.

[19]Hall, K. C. and Giovanetti, E. B., "Minimum Power Requirements and Optimal Rotor Design for Conventional and Compound Helicopters Using Higher Harmonic Control," American Helicopter Society 69th Annual Forum, Phoenix, AZ, 2013.

[20]Giovanetti, E. B. and Hall, K. C., "Optimum Design of Compound Helicopters Using Higher Harmonic Control," AHS 70th Annual Forum, 2014.

[21]Giovanetti, E. B. and Hall, K. C., "A Variational Approach to Multipoint Aerodynamic Optimization of Conventional and Coaxial Helicopter Rotors," AHS 71st Annual Forum, 2015.

[22]Yeo, H. and Johnson, W., "Investigation of Maximum Blade Loading Capability of Lift-Offset Rotors," *Journal of the American Helicopter Society*, Vol. 59, (012005), 2014.
doi: 10.4050/JAHS.59.012005

[23]Johnson, W., "Influence of Lift Offset on Rotorcraft Performance," AHS Specialist's Conference on Aeromechanics, San Francisco, CA, January 23-25, 2008.

[24]Floros, M. W. and Johnson, W., "Performance Analysis of the Slowed-Rotor Compound Helicopter Configuration," *Journal of the American Helicopter Society*, Vol. 54, (2), April 2009, pp. 1–12.
doi: 10.4050/JAHS.54.022002

[25]Floros, M. W. and Johnson, W., "Stability and Control Analysis of the Slowed-Rotor Compound Helicopter Configuration," *Journal of the American Helicopter Society*, Vol. 52, (3), Jul 2007, pp. 239– –253.
doi: 10.4050/JAHS.52.239

[26]Kim, H. W. and Brown, R. E., "Coaxial Rotor Performance and Wake Dynamics in Steady and Manoeuvering Flight," American Helicopter Society 62nd Annual Forum, 2006.

[27]Kim, H. W., Kenyon, A. R., Brown, R. E., and Duraisamy, K., "Interactional Aerodynamics and Acoustics of a Hingeless Coaxial Helicopter with an Auxiliary Propeller in Forward Flight," *The Aeronautical Journal*, Vol. 113, (1140), Feb 2009, pp. 65–78.

[28]Ferguson, K. and Thompson, D., "A Performance Analysis of Compound Helicopter Configurations," AHS 70th Annual Forum, Montreal, Canada, May 2014.

[29]Ferguson, K. and Thomson, D., "Flight Dynamics Investigation of Compound Helicopter Configurations," *Journal of Aircraft*, Vol. 52, 2015, pp. 156–167.
doi: 10.2514/1.C032657

[30]Sekula, M. K. and Gandhi, F., "Effects of Auxiliary Lift and Propulsion on Helicopter Vibration Reduction and Trim," *Journal of Aircraft*, Vol. 41, (3), May 2004, pp. 645–656.

[31]Sekula, M. K. and Gandhi, F., "Helicopter Vibration Reduction using Fixed-System Auxiliary Moments," *AIAA Journal*, Vol. 42, (3), March 2004, pp. 501 – 512.

[32]Sekula, M. K. and Gandhi, F., "Helicopter Vibration and Rotor Power Reduction through Horizontal Tail Incidence Angle Control," American Helicopter Society 60th Annual Forum, Baltimore, MD, June 2004.

[33]Gandhi, F. and Sekula, M. K., "Helicopter Horizontal Tail Incidence Control to Reduce Rotor Cyclic Pitch and Blade Flapping," American Helicopter Society 60th Annual Forum, Baltimore, MD, June 2004.

[34]Barron, H. M., Brentner, K., Hornand, J. F., Ozdemir, G., and Throsen, A., "Acoustic Analysis of Compound Helicopters with Trim Variations," American Helicopter Society 69th Annual Forum, Phoenix, AZ, May 2013.

[35]Reddinger, J.-P. and Gandhi, F., "A Physics-Based Approach to Trim Optimization of an Articulated Slowed-Rotor Compound Helicopter in High-Speed Flight," 70th American Helicopter Society Annual Forum, 2014.

[36]Jacobellis, G., Gandhi, F., and Floros, M. W., "A Physics-Based approach to Trim Optimization of Coaxial Rotors in High-Speed Flight," AHS 71st Annual Forum, 2015.

[37]Saberi, H., Khoshlahjeh, M., Ormiston, R., and Rutkowski, M., "Overviewof RCAS and Application toAdvanced Rotorcraft Problems," AHS Fourth Decennial Specialists Conference on Aeromechanics, San Francisco, CA, Jan 2004.

[38]Passe, B., Sridharan, A., Baeder, J., and Singh, R., "Identification of Rotor-Fuselage Aerodynamic Interactions in a Compound Coaxial Helicopter using CFD-CSD Coupling," AHS technical meeting on Aeromechanics Design for Vertical Lift, January 2016.

[39]Johnson, W., "Lift-Offset Compound Design Background, X2TD, JMR ME1A Status and Plans," , August 2011.

[40]Carter Aviation Technologies, "CarterCopter Brochure," , June 2015.